Article

Active Control of Low-Frequency Sound Transmission Using Force Radiation Modes: A Numerical Study

Rongfu Mao, Qiwei He, Shanping Gao* and Xiangrong Xie

School of Mechanical and Electrical Engineering, Quanzhou University of Information; Quanzhou 362000, China

* Correspondence: maorfu@163.com

Abstract

Active control is a highly effective method for mitigating low-frequency noise transmission. To address the coupling effect and practical implementation challenges associated with conventional active control methods, a specific strategy for active control of noise transmission is developed. By leveraging an intuitive representation of transmitted sound power through force radiation modes, the control forces are designed such that the total excitation force vector becomes orthogonal to each dominant force radiation mode. Detailed theoretical development and case studies are presented. The research results indicate that decoupled control of transmitted sound power corresponding to each force radiation mode can be achieved, and excellent control outcomes can be obtained in both oblique incident and diffuse field applications. Further investigations reveal that the noise transmission can be effectively reduced, while the total vibration attenuation on the plate may not be assured, which depends on the relationship that exists between dominant force radiation modes and corresponding structural modes.

Keywords: noise transmission; active control; force radiation modes; decoupling; low-frequency

1. Introduction

Contemporary high-end equipment is increasingly characterized by high speed, heavy loads, lightweight construction, and operation in extreme environments, which brings more serious structural vibration and noise problems. In particular, the effective mitigation of low-frequency noise transmission is an urgent problem to be solved.

According to the mass law of sound insulation, structures with high transmission loss are characterized by a high surface density, which can result in excessive weight, especially in the low-frequency region. Due to the demand for lightweight design and low cost, alternative approaches are considered in practice. Beyond widely adopted damping material installation, topology optimization, and composite structure design methods, several researchers have investigated the attachment of discrete rigid masses to plates [1], demonstrating that this approach can yield greater transmission loss than a simple uniform mass increase. The use of dynamic vibration absorbers attached to a primary structure to improve the noise insulation has also been widely investigated [2–4]. In these studies, various types of dynamic vibration absorbers have been proposed, with their resonance frequencies tuned to specific target frequencies to suppress structural vibrations and, consequently, reduce sound transmission. In recent years, advances in acoustic

Academic Editor:

Received: date
Revised: date
Accepted: date
Published: date

metamaterial theory have further enabled the development of actively tunable acoustic metamaterials, which have also been employed to improve sound transmission loss [5,6].

Active structural acoustic control (ASAC) is an effective acoustic control method that has minimal influence on the physical characteristics of the controlled structure, offering a significant advantage in achieving a satisfactory control effect in the low-frequency region. Therefore, studies and solutions on sound insulation with ASAC have been increasingly predominant. An analytical and experimental investigation of active control of sound transmission through double-panel systems was conducted by Carneal using the ASAC method [7]. Maamoun proposed a novel ASAC strategy for transparent-patched vibrating plates, achieving enhanced noise reduction and offering new insights into how actuator configuration influences acoustic performance [8]. Leveraging the principle that structural vibration can be decoupled from acoustic radiation, numerous researchers have extensively explored ASAC approaches based on Acoustic Radiation Modes (ARMs), yielding many significant and constructive results [9–11].

From the perspective of control objectives, existing ASAC research can be broadly classified into two categories: structural mode (SM)-based control and ARM-based control. In SM-based ASAC methods, noise reduction is not guaranteed due to the inherent coupling between structural modes and radiated sound power. In contrast, ARM-based approaches enable decoupled control of radiated acoustic power; however, they do not provide an intuitive means to determine the spatial distribution of the required control forces, which presents practical challenges for implementation.

Yamaguchi [12,13] introduced a structural admittance matrix to extend the concept of ARM to Force Radiation Mode (FRM), asserting that the FRM method provides the most effective framework for analyzing the relationship between excitation force distribution and radiated sound power. Based on this approach, Ji employed FRMs to investigate the influence of excitation forces on structural sound radiation and to inform the design of low-noise structures [14,15]. Since the radiated sound power is expressed by the excitation force as the variable, FRMs offer a more intuitive representation of the relationship between the excitation force and the transmitted sound power, facilitating the determination of control force distribution requirements in ASAC. Building upon these merits, the authors previously introduced FRMs into ASAC for acoustic radiation problems [16]. In this paper, the FRM framework is extended to the domain of noise transmission, and a specific active control strategy is developed, which is implemented and evaluated through rigorous case studies.

2. Theoretical development

2.1. Concept of force radiation mode

Consider an arbitrary vibrator structure immerged in homogeneous fluid with sound velocity c_0 and density ρ_0, and the structure vibrates harmonically and creates reflected and transmitted sound waves in the upper and lower half-spaces at frequency ω, respectively. The vibrating surface is discretized into N elements, and all distributed acoustical quantities are represented by corresponding samplings at the centers of each discretized element.

The surface pressure vector $\mathbf{p}$ can be expressed by the normal velocity vector $\mathbf{v}_\mathrm{n}$ ($e^{j\omega t}$ is assumed for a simple form)

$$\mathbf{p} = \mathbf{Z}\mathbf{S}\mathbf{v}_\mathrm{n} = (\mathbf{R}' + j\mathbf{X}')\mathbf{S}\mathbf{v}_\mathrm{n}, \tag{1}$$

where, $j = \sqrt{-1}$, $\mathbf{p}$ and $\mathbf{v}_\mathrm{n}$ are $(N \times 1)$ vectors of surface pressure and normal velocity on the discretized vibrating boundary surface, respectively, S is an $(N \times N)$ diagonal matrix with area of the i-th element $s_i (i = 1,2,\dots,N)$ in the diagonal position, $\mathbf{Z}$ is an $(N \times N)$ impedance matrix of the vibrating structure surface with real part matrix $\mathbf{R}'$ and imaginary part matrix $\mathbf{X}'$, and it is always derived by the Boundary Element Method (BEM) procedure and other numerical methods.

The transmitted sound power W_t can be obtained by surface pressure $\mathbf{p}$ and normal velocity $\mathbf{v}_\mathrm{n}$

$$W_t = \frac{1}{4}[\mathbf{p}^\mathrm{T}\mathbf{S}\mathbf{v}_\boldsymbol{n}^* + \mathbf{p}^\mathrm{H}\mathbf{S}\mathbf{v}_\mathrm{n}], \tag{2}$$

where, superscript "*", "T" and "H" denote conjugate transpose and conjugate transpose operator respectively.

Substituting Equation (1) into Equation (2), the transmitted sound power W_t can be obtained as

$$W = \frac{1}{2}\mathbf{v}_\mathbf{n}^\mathrm{H}\mathbf{S}\mathbf{R}'\mathbf{S}\mathbf{v}_\mathbf{n} = \mathbf{v}_\mathbf{n}^\mathrm{H}\mathbf{R}\mathbf{v}_\mathbf{n}, \tag{3}$$

where $\mathbf{R}=\mathbf{S}\mathbf{R}'\mathbf{S}/\mathbf{2}$, which is an $(N \times N)$ real symmetric matrix. For the plate radiators in a baffle, this radiation matrix can be calculated analytically,

$$R=\frac{k^2\rho c}{4\pi}\begin{bmatrix} s_1 s_1 & \frac{s_1 s_2 \sin kr_{12}}{kr_{12}} & \cdots & \frac{s_1 s_N \sin kr_{1N}}{kr_{1N}} \\ \frac{s_2 s_1 \sin kr_{21}}{kr_{21}} & s_2 s_2 & \cdots & \frac{s_2 s_N \sin kr_{2N}}{kr_{2N}} \\ \cdots & \cdots & \cdots & \cdots \\ \frac{s_N s_1 \sin kr_{N1}}{kr_{N1}} & \frac{s_N s_2 \sin kr_{N2}}{kr_{N2}} & \cdots & s_N s_N \end{bmatrix} \tag{4}$$

in which r_{mn} is the distance from element m to element n, and $k = \omega/c_0$ is the wave number.

The relationship between the normal velocity $\mathbf{v}_\mathbf{n}$ and the excitation force vector $\mathbf{F}$ can be expressed as

$$\mathbf{v}_\mathbf{n} = \mathbf{Q}\mathbf{F}, \tag{5}$$

where $\mathbf{Q}$ is the $(N \times N)$ structural admittance matrix, by which the structural-acoustic interaction can be counted comprehensively. According to the modal analysis theory, the matrix $\mathbf{Q}$ of the plate vibrating in the air can be expressed by approximately

$$Q(m,n) = j\omega \sum_{i=1}^{\infty} \frac{\Phi_i(m)\Phi_i(n)}{m_i(\omega_i^2(1+j\eta_i) - \omega^2)} \tag{6}$$

where Φ_i is the mode shape vector, m_i is the modal mass, ω_i and η_i are the modal frequency and damping loss factor, respectively. The subscript i denotes the mode order number.

Substituting Equation (5) into Equation (3), the transmitted sound power W_t can be rewritten as

$$W_t = \mathbf{F}^{\mathrm{H}}\mathbf{Q}^{\mathrm{H}}\mathbf{R}\mathbf{Q}\mathbf{F} = \mathbf{F}^{\mathrm{H}}\mathbf{T}\mathbf{F}, \tag{7}$$

where $\mathbf{T} = \mathbf{Q}^{\mathrm{H}}\mathbf{R}\mathbf{Q}$, which is an $(N \times N)$ Hermitian matrix. From the physical definition of the acoustic power W_t in Equation (7), it can be deduced that $W_t > 0$ will always be true except when the excitation force vector equals $\mathbf{0}$. Therefore, $\mathbf{T}$ is positive definite and Hermitian, and it can be expressed by the eigenvalue decomposition as

$$\mathbf{T} = \mathbf{D}\mathbf{A}\mathbf{D}^{\mathrm{H}}, \tag{8}$$

where $\mathbf{A}$ is a diagonal matrix with eigenvalues $\lambda_i (i = 1,2,\dots,N)$ decreasing monotonically along the diagonal, $\mathbf{D}$ represents an $(N \times N)$ matrix whose columns are eigenvectors $\mathbf{d}_i (i = 1,2,\dots,N)$. Since $\mathbf{T}$ is positive definite and Hermitian, all of its eigenvalues λ_i are positive real, and its eigenvectors $\mathbf{d}_i$ are orthogonal to each other. Each eigenvector $\mathbf{d}_i$ represents a particular excitation force pattern on the vibrating surface, so it's termed as Force Radiation Mode specifically.

From Equation (7), the matrix $\mathbf{T}$ depends on $\mathbf{Q}$ and $\mathbf{R}$. By the definition, $\mathbf{Q}$ is related to the stiffness matrix and mass matrix of the structure, while $\mathbf{R}$ is related to the geometry of the vibrating surface and excitation frequency. Therefore, FRMs are not only dependent on the geometry and excitation frequency but also on the material properties and boundary conditions of the flexible structure.

2.2. Transmitted Noise and Transmission Loss

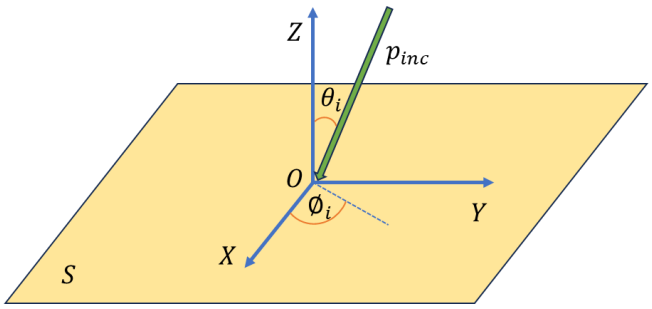

Figure 1. Illustration of the incidence wave and coordinates

For the noise transmission problem, as illustrated in Figure 1, assume an oblique plane sound wave p_{inc} varying harmonically is incident upon the structure with elevation angle θ_i and azimuth angle $\emptyset_i$, and the amplitude P_0

$$p_{\mathrm{inc}}(x,y,z) = P_0 e^{-j(k_x x + k_y y + k_z z)}, \tag{9}$$

where $k_x = k_0 sin\theta_i cos\emptyset_i$, $k_y = k_0 sin\theta_i sin\emptyset_i$, $k_z = k_0 cos\theta_i$, and $k_0 = \omega/c_0$.

Substituting Equation (8) into Equation (7), the transmitted sound power W_t becomes

$$W_t = \mathbf{F}^{\mathrm{H}}\mathbf{D}\mathbf{A}\mathbf{D}^{\mathrm{H}}\mathbf{F} = \mathbf{y}\mathbf{A}\mathbf{y}^{\mathrm{H}} = \sum_{i=1}^{N} \lambda_i |y_i|^2, \tag{10}$$

where $\mathbf{y} = \mathbf{F}^{\mathrm{H}}\mathbf{D}$, which is the amplitude coefficient vector of FRM, and the excitation force vector $\mathbf{F}$ can be determined by

$$\mathbf{F} = \mathbf{S}\mathbf{p}_{\mathrm{b}}, \tag{11}$$

where $\mathbf{p}_{\mathrm{b}}$ is the blocked pressure vector with each element equals $2p_{\mathrm{inc}}$[3,17].

As can be seen from Equation (10), the total transmitted sound power is the sum of corresponding components of each order of FRM, and there is no coupling behavior between each FRM. Therefore, the transmitted sound power can be decoupled and controlled effectively via the independent FRMs.

The power that is incident on the structure is given by

$$W_i = \iint P_0^2 \cos(\theta_i)/(2\rho_0 c_0)\, dS, \tag{12}$$

Finally, the transmission loss TL can be obtained by the oblique sound power transmission coefficient $\tau(\theta_i, \emptyset_i)$

$$TL = 10\log_{10}(1/\tau(\theta_i, \emptyset_i)) = 10\log_{10}(W_i/W_t), \tag{13}$$

2.3. Strategy of active control

For active control of noise transmission, supposing the total excitation force distribution on the flexible structure is composed of an oblique plane sound wave p_{inc} and secondary control forces $\mathbf{F}_s$

$$\mathbf{F} = \mathbf{S}\mathbf{p}_{\mathrm{b}} + \mathbf{F}_s, \tag{14}$$

It can be seen from the observation of Equation (10) that perfect control can be obtained if the FRM amplitude coefficient vector $\mathbf{y}$ can be set to $\mathbf{0}$. To satisfy this condition, an intuitive active control principle can be formed, on which the total excitation force vector $\mathbf{F}$ is orthogonal to each dominant FRM by assigning a certain secondary control force distribution. In practical applications, since the first several eigenvalues in Equation (10) are far larger than others, the transmitted sound power would mainly be contributed by the corresponding dominant FRMs, and the amplitude coefficient vector $\mathbf{y}$ can be expressed approximately by

$$\mathbf{y} \approx (\mathbf{S}\mathbf{p}_{\mathrm{b}} + \mathbf{F}_s)^{\mathrm{H}}[\mathbf{d}_1 \ldots \mathbf{d}_k], \tag{15}$$

where $\mathbf{d}_1, \ldots, \mathbf{d}_k$ are the first k dominant FRMs.

If the amplitude of $\mathbf{y}$ in Equation (15) is driven to $\mathbf{0}$, the desired secondary control forces $\mathbf{F}_s$ can be expressed as

$$\mathbf{F}_s = -\left(\mathbf{D}_k{}^{\mathrm{H}}\right)^{+}\mathbf{D}_k{}^{\mathrm{H}}\mathbf{S}\mathbf{p}_{\mathrm{b}}, \tag{16}$$

where $\mathbf{D}_k = [\mathbf{d}_1 \ldots \mathbf{d}_k]$, and superscript "+" denotes pseudo inverse operator. Note that eigenvectors $\mathbf{d}_i$ are orthogonal to each other, the matrix $\mathbf{D}_k$ is an orthonormal matrix, and its condition number is 1. In practice, Equation (16) can be solved by an adaptive control algorithm.

Therefore, a strategy of active control based on FRM theory is summarized as follows:

(1) Discretize the vibrating surface of the flexible structure, and perform the eigenvalue decomposition according to Equation (8) to obtain eigenvectors and eigenvalues.

(2) Determine the first k dominant FRMs by a certain criterion, e.g., $\lambda_i/\lambda_1 > 0.01$.

(3) Calculate amplitude coefficients of the dominant FRMs.

(4) Set the square sum of amplitude coefficients as the control objective function.

(5) Arrange secondary control forces according to the discretized grids, and adjust them to minimize the objective function in Equation (15) by direct matrix calculation using Equation (16) or an alternative adaptive control algorithm.

3. Case studies

Consider an acoustic plane wave incident on a rectangular plate as shown in Figure 1. The density of the air medium ρ_0 is 1.21 kg/m^3, and the sound velocity c_0 is 343 m/s. For the low-frequency noise transmission problem, the dimensions of the plate are comparable to the large sound wavelengths, and the plate is modeled as simply supported in an infinite baffle. Key parameters of the plate are listed in Table 1, and the first six structural modal frequencies are shown in Table 2.

Table 1. Key parameters of the plate

Item	Value	Unit
Density ρ	2700	kg/m^3
Young's modulus E	70	Pa
Poisson's ratio ν	0.33	/
Loss factor η	0.004	/
Width L_x	0.38	m
Length L_y	0.15	m
Thickness h	0.81	mm

Table 2. The first 6 structural modal frequencies

Order	(1,1)	(1,2)	(1,3)	(1,4)	(2,1)	(2,2)
Modal frequency /Hz	101.8	142.9	211.5	307.6	365.9	407.1

3.1. FRM calculations

According to the theoretical development described in this paper, FRM calculations are performed at representative modal and non-modal frequencies. The amplitude distributions of the first four FRMs at (1,1), (1,2), (2,2) modal frequencies and non-modal frequency of 390Hz are illustrated in Figure 2(a)~(d), respectively. It can be seen that each order of FRM will change significantly at different frequencies. At the modal frequencies of the plate, the 1st FRM exhibits high consistency with the corresponding SM, and the higher-order FRMs resemble the SMs at adjacent modal frequencies. However, at the non-modal frequencies, the FRMs are not necessarily similar to the SMs at the adjacent modal frequencies.

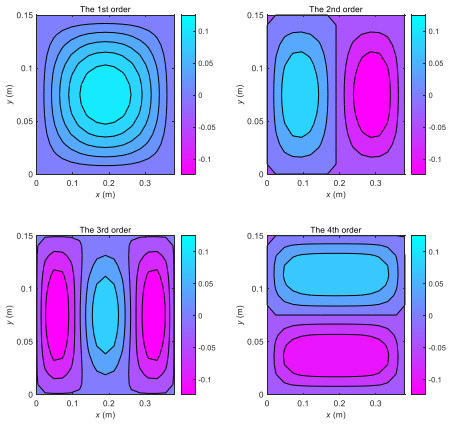

a) At (1,1) modal frequency

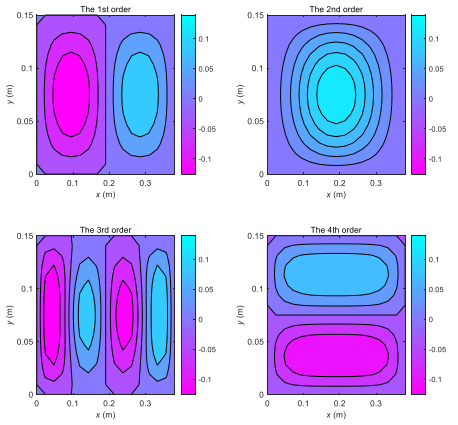

b) At (1,2) modal frequency

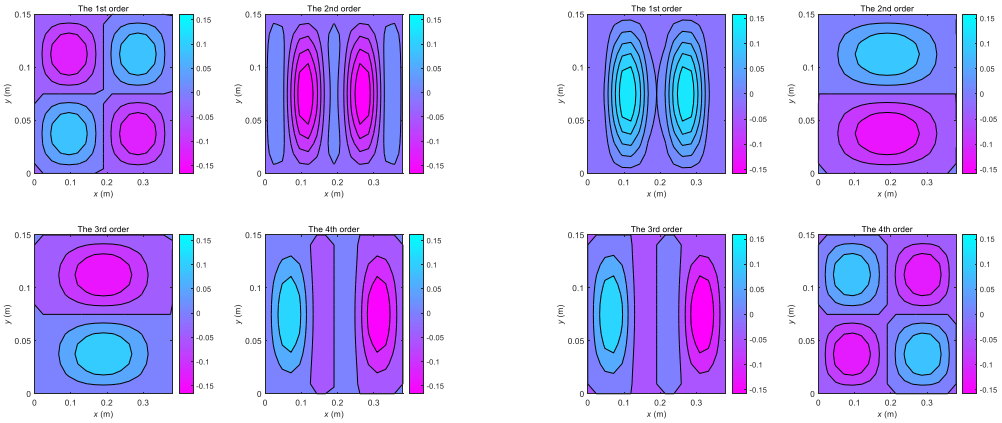

c) At (2,2) modal frequency d) At non-modal frequency 390Hz

Figure 2. The FRM amplitude distributions at typical frequencies

Figure 3 gives the first six eigenvalues of the plate varying with frequency. As can be seen, after mathematical eigenvalue decomposition, the eigenvalues corresponding to the 1st FRM are always the largest, and exhibit peak values at each modal frequency. The eigenvalues corresponding to the higher-order FRMs decrease with increasing order. At odd-odd modal frequencies, the eigenvalues corresponding to the higher-order FRMs decrease the most with increasing order, followed by odd-even (even-odd) modal frequencies. Meanwhile, at even-even and non-modal frequencies, the eigenvalues may decrease much more slowly. The above results reveal that it is sufficient to consider the contribution of the 1st or a first few dominant FRMs in the active control at odd-odd and odd-even (even-odd) modal frequencies, whereas more FRMs may need to be considered at even-even and non-modal frequencies.

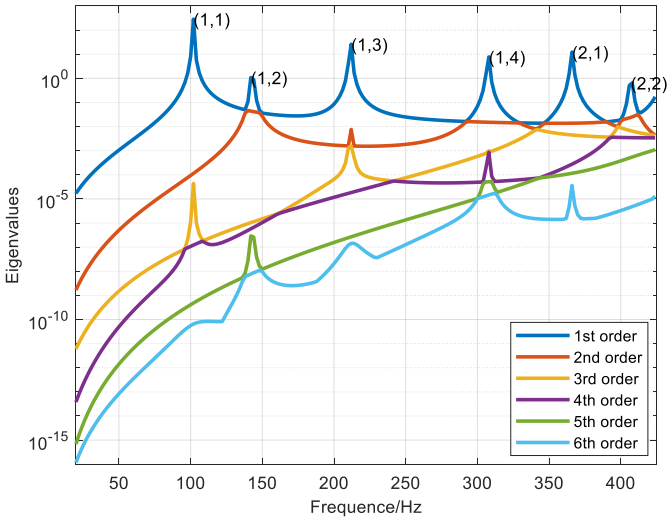

Figure 3. The eigenvalues corresponding to the first 6 FRMs

3.2. Calculation of transmitted noise and transmission loss

Assume an oblique plane wave is incident on the plate at $\theta_i = 30^\circ$ and $\emptyset_i = 45^\circ$, and the oblique incidence transmitted sound power W_t in Equation (10) is estimated by discretizing the structure surface. Since the estimation accuracy is determined by the mesh size, the convergence of estimation accuracy is checked first. To measure convergence of

estimation accuracy, an error indicator E is defined by Equation (17), in which the reference values $W_0(f)$ are calculated with a dense enough grid 41×21.

$$E = \sqrt{\frac{\sum_f |W_t(f) - W_0(f)|^2}{\sum_f |W_0(f)|^2}} \times 100\%, \quad (17)$$

Table 3. Mesh grid sizes

No.	S1	S2	S3	S4	S5
Grid sizes	9×5	13×7	17×9	21×11	25×13

The plate is divided evenly into different mesh grids, as shown in Table 3, and the error indicator E is calculated. The convergence results in the resonance-controlled frequency band 20Hz-1000Hz are illustrated in Figure 4, which shows that the estimation accuracy is improved gradually with a denser grid, and satisfactory convergence to the reference values is observed. For a balance of estimation accuracy and implementation efforts, a mesh grid 17×9 is desirable for subsequent analysis of the plate.

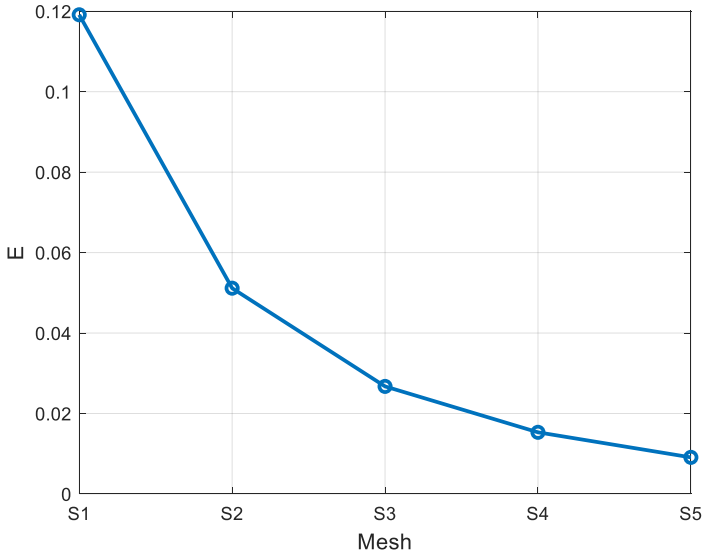

Figure 4. Estimation accuracy of different mesh grids

The accuracy validation of the transmitted sound power estimation with the presented active control strategy is then conducted. The oblique transmitted sound power and transmission loss at $\theta_i = 30^\circ$ and $\emptyset_i = 45^\circ$ are calculated by the presented method via Equation (10) and by the analytic method [17]. Corresponding transmitted sound power and transmission loss are compared in Figure 5 and Figure 6, respectively. As can be seen from the figures, the results estimated by the presented method coincide well with those by the analytic method in general, especially in the low-frequency band. However, a moderate growing discrepancy trend is also observed with increasing frequency, which is due to the fact that the accuracy of the present method is restricted by the mesh grid size more obviously at higher frequencies. Considering that active control problems of noise transmission in practice mainly appear in the low-frequency region, the accuracy of the presented method is deemed sufficient.

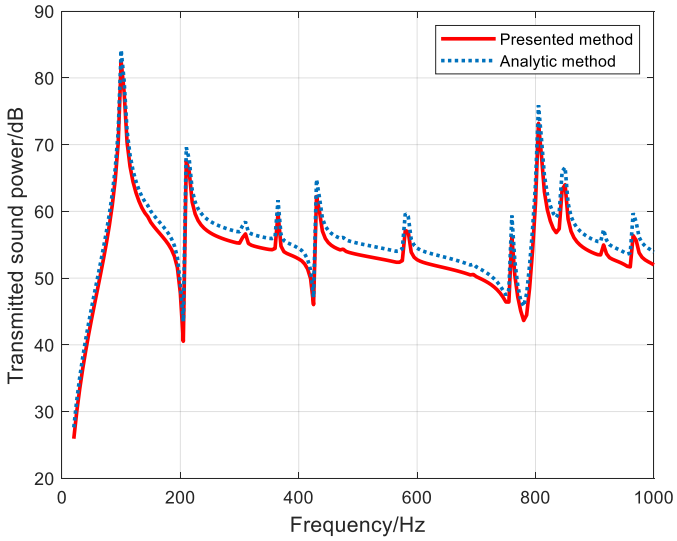

Figure 5. Comparison of the oblique transmitted sound power ($\theta_i = 30^\circ, \emptyset_i = 45^\circ$)

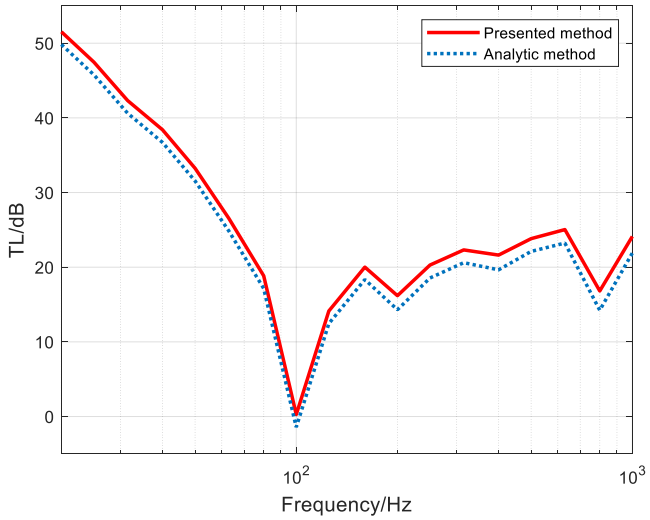

Figure 6. Comparison of the oblique transmission loss ($\theta_i = 30^\circ, \emptyset_i = 45^\circ$)

3.3. Active control results

Without loss of generality, two active control implementations are conducted, in which the transmitted sound contributed by the 1st FRM (termed as Control 1) and the first two FRMs are controlled (termed as Control 2) respectively. In addition to the oblique transmission loss *TL*, insertion loss *IL* is also adopted as a control effect indicator to demonstrate the performance of active control, which is defined as

$$IL = TL - TL_0, \tag{18}$$

where TL_0 is the oblique transmission loss without any control.

The oblique transmission loss and insertion loss are obtained with the presented strategy of active control, and the results are shown in Figures 7 and 8. Detailed results at typical resonant frequencies and non-resonant frequency of 390Hz are given in Table 4. As can be seen from the results, control of the 1st FRM contributed transmitted sound power in Control 1 can already achieve satisfactory reduction results at low frequency region, especially at the major resonant frequencies, e.g., the insertion loss at the (1,1) resonant frequency is up to 76.8dB. When the first two FRMs are controlled in Control 2, the

reduction of transmitted sound power is improved further over a wider frequency range, e.g., the insertion loss at the (1,2) order resonant frequency is increased substantially from 2.6dB to 63.1dB. The observations are due to the fact that transmitted sound power is mainly contributed by the first few dominant FRMs at these frequencies.

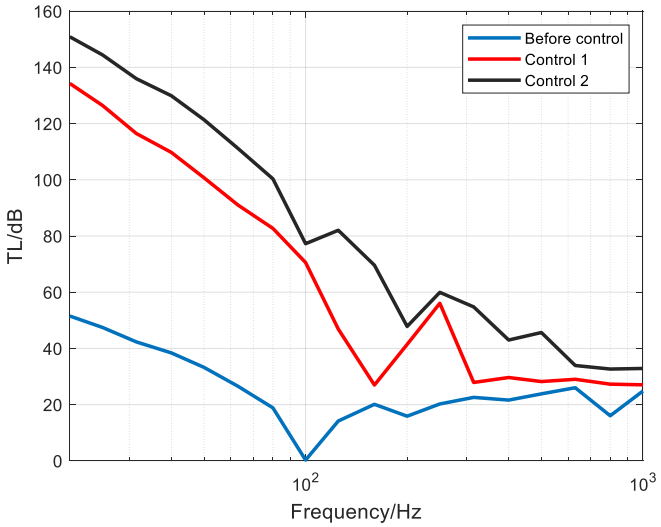

Figure 7. Results of the oblique transmission loss ($\theta_i = 30^\circ, \emptyset_i = 45^\circ$)

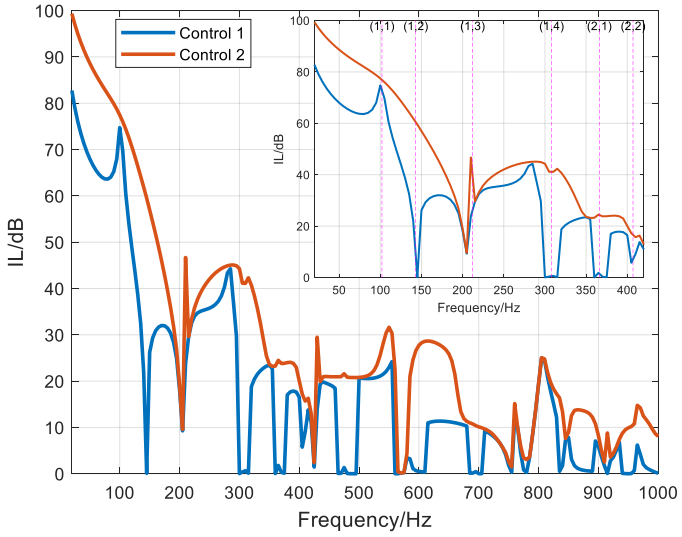

Figure 8. Results of the oblique insertion loss ($\theta_i = 30^\circ, \emptyset_i = 45^\circ$)

Table 4. Insertion loss at typical frequencies

Modal order /Frequency	(1,1)	(1,2)	(1,3)	(1,4)	(2,1)	(2,2)	390Hz
IL /dB (Control 1)	76.8	2.6	26.6	3.9	3.9	16.7	17.8
IL /dB (Control 2)	85.6	63.1	57.1	36.0	25.8	0.1	23.8

The diffuse field behavior of the presented strategy of active control is also investigated. The diffuse field on the source side can be designed as a sum of N_p uncorrelated plane waves moving in random directions.

$$p_{\mathrm{inc},diff} = \frac{P_0}{\sqrt{2N_p}} \sum_{n=1}^{N_p} e^{-j(k_{n,x}x + k_{n,y}y + k_{n,z}z)} e^{j\Psi_n} \quad (19)$$

where $k_{n,x} = k_0 sin\theta_n cos\emptyset_n$, $k_{n,y} = k_0 sin\theta_n sin\emptyset_n$, $k_{n,z} = k_0 cos\theta_n$. The polar angles $0 \le \theta_n \le \pi/2$ and $0 \le \emptyset_n \le 2\pi$ as well as the phase $0 \le \Psi_n \le 2\pi$ are independent random numbers. The term $1/\sqrt{2N_p}$ ensures that the designed field has a constant intensity for any choice of N_p.

By replacing the oblique incident field in Equation (9) with the diffuse field in Equation (19), then the transmitted sound power and transmission loss for the diffuse field can be calculated with the present strategy. The results for large enough $N_p = 500$ are illustrated in Figure 9. It can be found that the diffuse field transmission loss curves resemble the above oblique results, except for slightly lower overall values in the low-frequency region, indicating that excellent control outcomes can still be achieved in diffuse field applications with the presented strategy of active control.

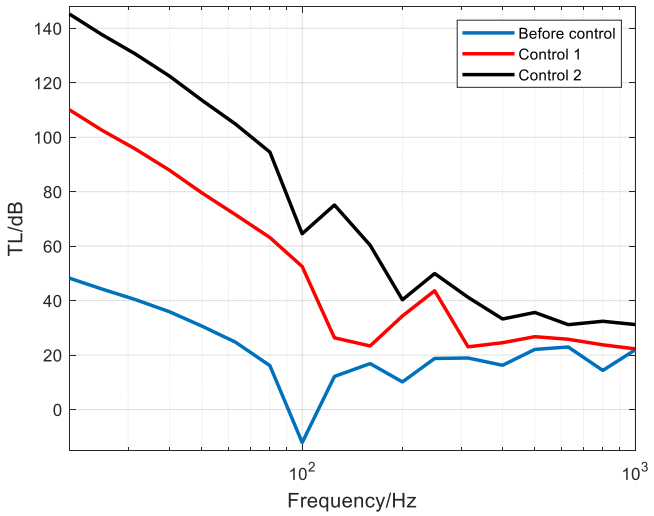

Figure 9. Results of the diffuse field TL before and after control

3.4. Implementation feasibility

The implementation feasibility of the presented control strategy is discussed through investigations of control performance and control force demand with grid size. Four grids termed as G1-G4 are prepared with the same 9 grids in the y direction and 3, 5, 9,17 grids respectively in the x direction.

Firstly, the secondary control forces are arranged according to the discretized grids G1-G4. To reveal the control performance of the presented control strategy with different arrangements clearly, the transmission loss results of all arrangements are evaluated on the same dense enough grid G4, then the insertion loss is calculated by using the transmission loss without active control as the reference result TL_0. The control performances of Control 1 case and Control 2 case in low-frequency regions are demonstrated in Figure 10(a) and Figure 10(b), respectively. It can be observed that the oblique insertion loss of grid G1 is not satisfactory due to insufficient control forces (3 grids), and the results increase gradually with denser grids G2-G4. Hence, it can be inferred that the influence of control force size on final control performance is similar to the rule of velocity sampling for sound radiation prediction [18], and the control force size is directly determined by the FRM distribution in the low-frequency region. By overall analysis of the results of G1-G4, the sampling interval should be less than half of the geometrical length of the FRM to guarantee reasonable control performance. Meanwhile, it can be noted that the insertion loss results are always positive except at two anti-resonate frequencies (i.e., 204Hz and 426Hz that correspond to transmission sound power dips in Figure 5), which means that additional transmission loss can be ensured as the requirement of control force size is satisfied.

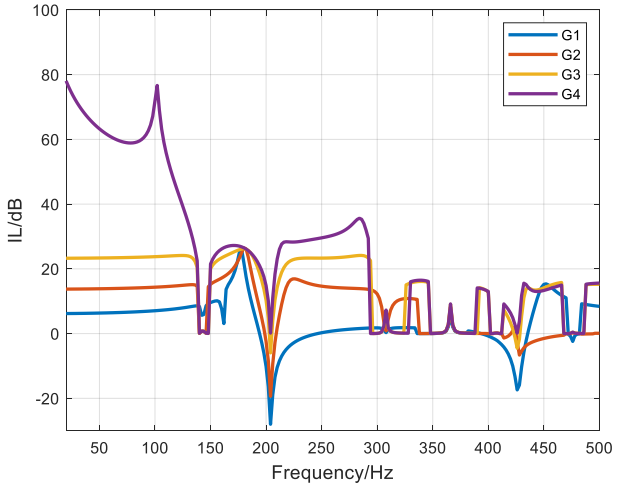

a) Control 1

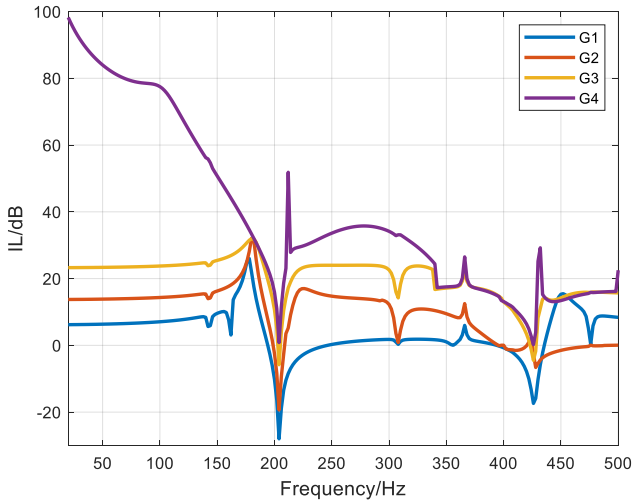

b) Control 2

Figure 10. Control performance of Control 1 and Control 2 with grid sizes

Moreover, the control effort is investigated, and it's represented by the amplitude ratio of the control force to the incident plane sound wave. The max ratio results of Control 1 case and Control 2 case are illustrated in Figure 11(a) and Figure 11 (b), respectively. It can be seen from the results that the max control force amplitudes are inversely proportional to the grid size generally, and the control forces are all within the feasible range of actuators. Therefore, the applicability of the presented strategy can be ensured in essence.

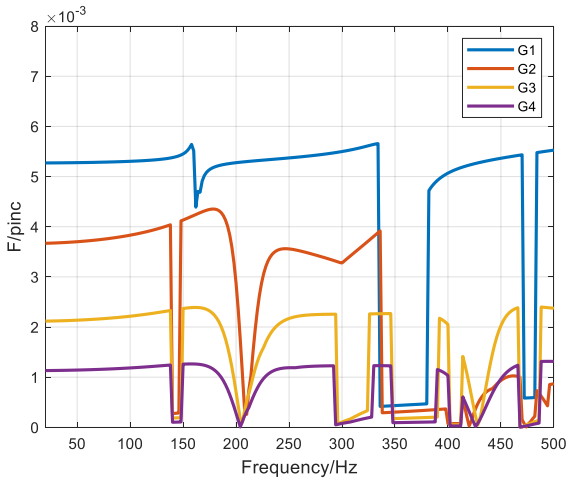

a) Control 1

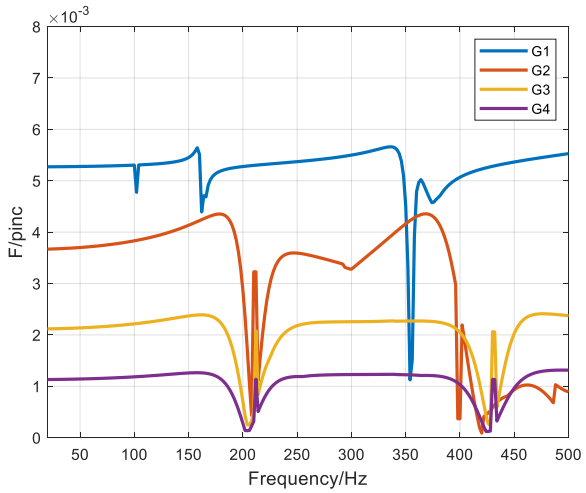

b) Control 2

Figure 11. Control effort of Control 1 and Control 2 with grid sizes

4. Further investigations

To demonstrate the performance of the presented strategy of active control more clearly, some active control cases at typical modal and non-modal frequencies in Table 4 are analyzed, and further investigations are conducted.

First, the control case at the (1,1) resonant frequency was examined. As can be seen from the detailed results in Table 4, a satisfactory control result can already be obtained when the 1st FRM is controlled. The amplitude comparison of FRMs and SMs before and after control is shown in Figure 12. Considering the fact that the amplitude of the 1st FRM before control is the largest one, as shown in Figure 10, and its eigenvalue is much higher than that of the higher order FRMs, as shown in Figure 3. Thus, the 1st FRM is the dominant FRM in this case [10]. It can be noted from Figure 12 (a) that the amplitude of the 1st FRM (dominant FRM) is reduced significantly after control, while the amplitudes of higher orders of FRMs remain almost unchanged. Therefore, the transmitted sound power can be effectively attenuated when the 1st FRM contributions are controlled. On the other hand, since the 1st FRM is similar to the SM near the modal frequency, the amplitude of (1,1) SM (contributing the most to the vibration before control) is also suppressed

significantly, as shown in Figure 12 (b), while the amplitudes of other SMs are still nearly unaltered. Therefore, the vibration on the plate can also be well controlled. This inference is confirmed by the vibration velocity distributions on the plate illustrated in Figure 13. It can be observed that the vibration velocity of the plate is changed and drastically attenuated after control, and the RMS value of the vibration velocity decreases from 144.8mm/s before control to 0.1mm/s after control. Based on the above results, it can be deduced that the noise transmission and vibration of the plate can both be attenuated effectively at resonant frequencies when dominant FRMs are controlled with the presented strategy, due to the similarity between dominant FRMs and corresponding SMs.

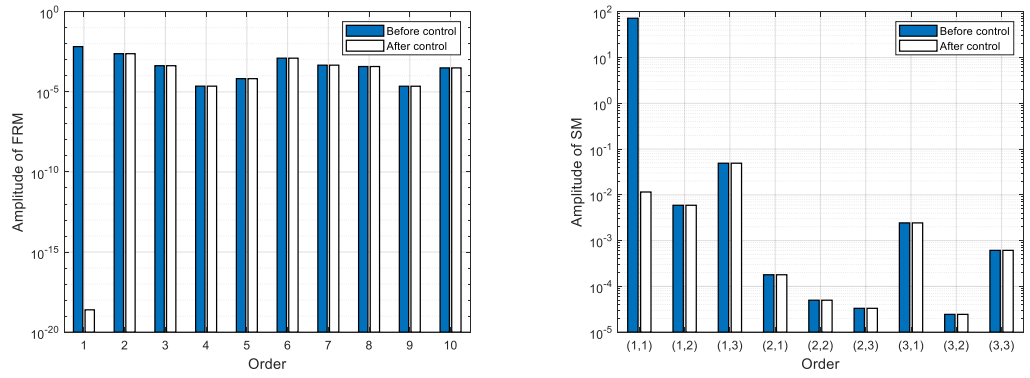

a） Amplitude of FRMs b） Amplitude of SMs

Figure 12. Comparison of amplitudes of FRMs and SMs at (1,1) resonant frequency

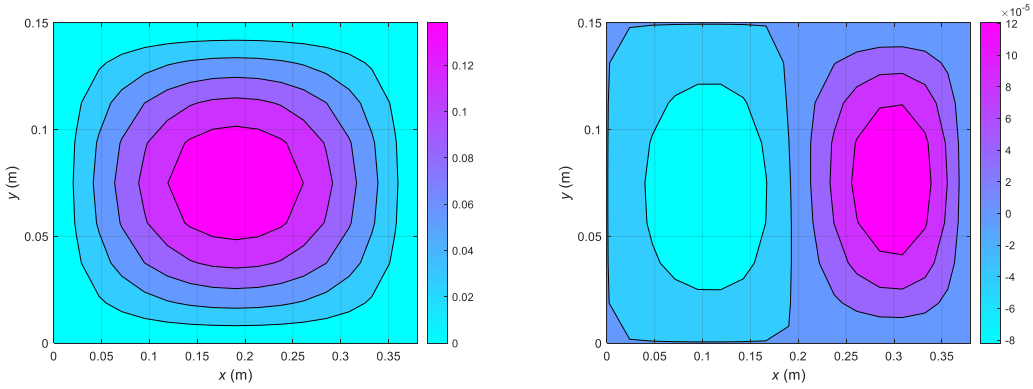

a） before control b） after control

Figure 13. The vibration velocity distributions on the plate at (1,1) resonate frequency

Next, the control case at the non-modal frequency of 390Hz is investigated. As can be seen from the results in Table 4, the insertion loss is about 17.8dB for Control 1 and 23.8 dB for Control 2. The amplitude comparison of FRMs and SMs before and after control (Control 2) is shown in Figure 12. Similar to the above analysis of the amplitudes of FRM and corresponding eigenvalues, the first two FRMs are the dominant FRMs in this case. As can be found in Figure 14(a), the amplitudes of the first two FRMs (dominant FRM) are reduced significantly after control. However, the amplitudes of SMs show different behaviors after control as shown in Figure 14 (b), i.e., amplitudes of some SMs (e.g., (1,1), (1,2), (1,3) modes) are suppressed more or less, while others (e.g., (2,2), (3,1) modes) become even larger by contrary. Therefore, the total vibration on the plate may not be attenuated subsequently, the reason is that dominant FRMs are not necessarily similar to adjacent SMs at non-modal frequencies. Final vibration velocity distributions on the plate are

shown in Figure 15. It's seen that the vibration distribution is also changed and the level is even increased after control to a certain extent, with the RMS value of the vibration velocity increased from 0.37mm/s before control to 0.62mm/s after control. By integrating the above analysis, it can be inferred that noise transmission of the plate can also be controlled effectively when dominant FRMs are controlled, while the total vibration attenuation on the plate may not be assured yet at non-modal frequencies, due to the complex relationship that exists between dominant FRMs and corresponding SMs. It is worth mentioning that in practical application, if the vibration amplification is too obvious to result in other possible influences such as structure strength and fatigue, remedies incorporating vibration constraints or employing multi-objective optimization should be considered.

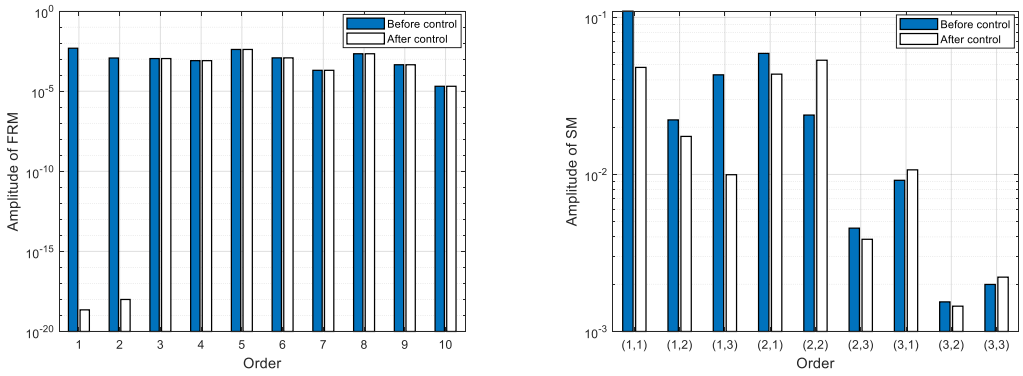

a） Amplitude of FRMs b） Amplitude of SMs

Figure14. Comparison of amplitudes of FRMs and SMs at 390Hz

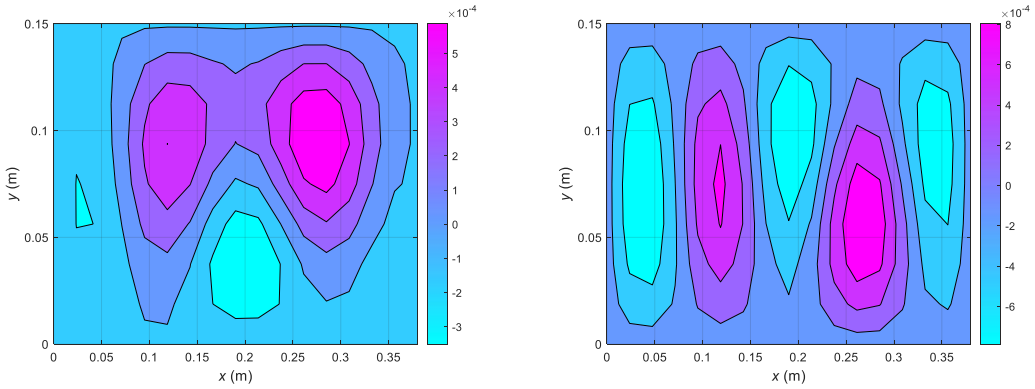

a） before control b） after control

Figure 15. The vibration velocity distributions on the plate at 390Hz

5. Conclusions

By virtue of the intuitive representation of the relationship between excitation force and transmitted sound power, the FRM framework has been successfully applied to the active control of noise transmission. The control forces are configured to make the total excitation force vector orthogonal to each dominant FRM, and a specific strategy for active control of noise transmission is developed. The following conclusions are drawn from the theoretical development and case studies:

(1) At the modal frequencies of the plate, the 1st FRM exhibits high consistency with the corresponding SM, and the higher-order FRMs show similar modal shapes with the

SMs at adjacent modal frequencies. However, at the non-modal frequencies, the FRMs are not necessarily similar to the SMs at the adjacent modal frequencies.

(2) Decoupled control of transmitted sound power corresponding to each FRM can be achieved, yielding excellent performance in both oblique incident and diffuse field applications. This greatly simplifies the control system and enhances its effectiveness and robustness.

(3) Noise transmission can be effectively reduced, while the total vibration attenuation on the plate may not be assured, which depends on the relationship that exists between dominant FRMs and corresponding SMs.

The presented strategy is anticipated to significantly simplify the control system and improve the control effect of noise transmission in practical applications. Further experimental validations will be conducted.

Author Contributions: Conceptualization, Rongfu Mao; Supervision, Qiwei He; Methodology, Shanping Gao; Validation, Xiangrong Xie. All authors have read and agreed to the published version of the manuscript.

Funding: This research was funded by the Natural Science Foundation of Fujian Province, China, grant number 2025J011606.

Data Availability Statement: The original contributions presented in this study are included in the article. Further inquiries can be directed to the corresponding author.

Conflicts of Interest: The authors declare no conflicts of interest.

References

1. Howard C.Q. Theoretical and Experimental Results of the Transmission Loss of a Panel with Discrete Masses Attached. In Proceedings of the 14th International Congress on Sound and Vibration, Cairns, Queensland, Australia, 9-12 July, 2007.
2. Howard C.Q. Transmission loss of a panel with an array of tuned vibration absorbers. *Acoust. Aust.* **2008**, vol.36, no.3, 98–103. https://doi.org/10.1016/j.jsv.2008.04.036.
3. Xiao Y.; Wen J.H.; Wen X.S. Sound transmission loss of metamaterial-based thin plates with multiple subwavelength arrays of attached resonators. *J. Sound Vib.* **2012**, vol.331, 5408-5423, https://doi.org/10.1016/j.jsv.2012.07.016.
4. Ajith A.; Balakrishnan B.; Raja S.; Paul V.S. Sound Transmission Performance of Plate-Type Acoustic Metamaterials for Quieter Aircraft Cabins. *Appl. Acoust.* **2025**, vol.238, 110806. https://doi.org/10.1016/j.apacoust.2025.110806.
5. Nouh M. A.; Aldraihem O. J.; Baz A. Periodic metamaterial plates with smart tunable local resonators. *J. Intell. Mater. Syst. Struct.* **2016**, vol. 27, 1829-1845. https://doi.org/10.1177/1045389X15615965.
6. Wang T.; Wang Y. Z. Active Feedback Control on Sound Transmission Loss of Metamaterial Shell. *AIAA J.* **2025**, vol.63, 1541-1559. https://doi.org/10.2514/1.J064271.
7. Carneal J. P.; Fuller C. R. An analytical and experimental investigation of active structural acoustic control of noise transmission through double panel systems. *J. Sound Vib.* **2004**, vol.272, 749-771. https://doi.org/10.1016/S0022-460X(03)00418-8.
8. Maamoun K. S. A.; Aboutiman A.; Ali M. A. Synergistic use of inertial actuators for advanced noise control in transparent-patched vibrating plates. *Measurement* **2026**, vol. 257, 118701. https://doi.org/10.1016/j.measurement.2025.118701.
9. Hesse C.; Papantoni V.; Algermissen S.; Monner H.P. Frequency-independent radiation modes of interior sound radiation: Experimental study and global active control. *J. Sound Vib.* **2017**, vol. 401, 204-213. https://doi.org/10.1016/j.jsv.2017.04.038.
10. Su C. W.; Zhu H. C.; Mao R. F. Determination method of dominant acoustic radiation modes in coupling enclosure (in Chinese). *J. Natl. Univ. Def. Technol.* **2019**, vol. 41, 158-162. https://doi.org/10.11887/j.cn.201902023.
11. Jeon O.; Kim H. G.; Kook J. H.; Kim S. M.; Wang S. Y. Active structural acoustic control for radiated sound power reduction of enclosure with vent holes based on radiation modes. *J. Mech. Sci. Technol.* **2022**, vol. 36, 1-5. https://doi.org/10.1007/s12206-022-0611-y.
12. Yamaguchi Z.; Bolton J. S.; Sakagami K. Reduction of sound radiation by using force radiation modes. *Appl. Acoust.* **2011**, vol. 72, 420-427. https://doi.org/10.1016/j.apacoust.2011.01.006.
13. Yamaguchi Z.; Sakagami K.; Morimoto M.; Bolton J. S. Experimental identification of force radiation modes. *Noise Control Eng. J.* **2013**, vol. 61, 81-86. https://doi.org/10.3397/1/1.3761008.

14. Ji G.; Zhang W. K.; Zhou Q. D.; Tan L. Force radiation mode analysis and acoustic reduction of cylindrical structure (in Chinese). *J. Naval. Univ. Eng*. **2014**, vol. 26, 83-87+91. https://doi.org/10.7495/j.issn.1009-3486.2014.04.020.
15. Fu L., Ji G.; Zhou Q. D.; Pan Y. C. The influence of driving force location on acoustic power radiated from a cylindrical shell (in Chinese). *Tech. Acoust.* **2017**, vol. 36, 104-109. https://doi.org/10.16300/j.cnki.1000-3630.2017.02.002.
16. Mao R. F.; Zhu H. C.; Gao S. P.; Zhang X. A Study on Active Structural Acoustic Control using Force Radiation Modes. *J. Vibroeng.* **2024**, Vol. 269, 1825–1835. https://doi.org/10.21595/jve.2024.24214.
17. Roussos L.A. Noise transmission loss of a rectangular plate in an infinite baffle. Technical report, NASA, Langley Research Center, Hampton, Virginia, USA, March 1985. NASA technical paper TP2398.
18. Tao J.C.; Ge H.L.; Qiu X.J. A new rule of vibration sampling for predicting acoustical radiation from rectangular plates. *Appl. Acoust.* 2006, vol. 67, 756–770. https://doi.org/ 10.1016/j.apacoust.2005.12.005